Opto-Electronic Advances

Supplementary information

September 2024, Vol. 7, No. 9

DOI: 10.29026/oea.2024.240040

An externally perceivable smart leaky-wave antenna based on spoof surface plasmon polaritons

Weihan Li[1,2], Jia Chen, Shizhao Gao, Lingyun Niu, Jiaxuan Wei, Ruosong Sun, Yaqi Wei, Wenxuan Tang[1,2]* and Tie Jun Cui[1,2]*

[1]State Key Laboratory of Millimeter Waves, Southeast University, Nanjing 210096, China; [2]Institute of Electromagnetic Space, Southeast University, Nanjing 210096, China.

*Correspondence: WX Tang, Email: wenxuant@seu.edu.cn; TJ Cui, Email: tjcui@seu.edu.cn

This file includes:

Supplementary information for this paper is available at https://doi.org/10.29026/oea.2024.240040

Open Access This article is licensed under a Creative Commons Attribution 4.0 International License.
To view a copy of this license, visit http://creativecommons.org/licenses/by/4.0/.

© The Author(s) 2024. Published by Institute of Optics and Electronics, Chinese Academy of Sciences.

Section 1: Theoretical calculations of the radiation pattern

When EM waves are expected to radiate into free space, there are two procedures in the design. The first step is the coupling from the spoof surface plasmon polariton (SSPPs) transmission line (TL) to the patches, and the second step is the radiation of EM waves from the patches into free space. In the first step, EM waves propagate along the SSPPs TL, and at different locations of the TL the phase is different. The phases brought in by SSPPs waveguide are denoted as Ψ_{-3}, Ψ_{-2}, Ψ_{-1}, Ψ_0, Ψ_1, Ψ_2, and Ψ_3, corresponding to the patches numbered from −3 to 3, respectively. Then the phase difference between the n-th patch and the middle patch can be deduced by

$$\Delta\psi_n = k_s n d \,, \tag{S1}$$

among them, k_s is the wave number of the SSPPs waveguide. And d is the distance between adjacent patches. This kind of phase difference can be regarded as the compensation to the phase needed in the second step. In the second step, beam scanning characteristic is embodied. When the radiation pattern is expected to have an emergence angle (θ in Fig. S1(a)), the EM waves from different patches should pass the optical paths of different lengths to the inclined wavefront. So there must be some compensation to make the phase variations via different optical paths own an equal value. The phase along the propagation direction are φ_{-3}, φ_{-2}, φ_{-1}, φ_0, φ_1, φ_2, and φ_3, corresponding to patches numbered from −3 to 3, respectively. Different φ_n needed in the beam scanning procedure at different frequencies are brought in the SSPPs waveguide, which is only cause of the beam scanning characteristic. If the scan angle is expected to be θ, that is to say, the angle between the constant phase front and the horizontal plane is θ, then the phase difference between the n-th patch and the middle patch can be deduced by $k_0\Delta s = -k_0 n d\sin\theta$, in which k_0 and Δs denote the propagation constant in the free space and the optical path difference, respectively and d is the distance between adjacent patches. As a consequence, the radiation patterns can be predicted by the following equation without considering the element factor:

$$E = C\frac{\mathrm{e}^{-\mathrm{j}kr}}{r}\int f(\theta,\varphi)\,S(\theta)\ \,, \tag{S2}$$

in which,

$$S(\theta) = \sum_{n=-3}^{3} I_n \mathrm{e}^{\mathrm{j}n\phi}\,, \tag{S3}$$

$$\varphi = k_0 d\sin(\theta)\ \,, \tag{S4}$$

where θ is the angle of the observation point, $\Delta\psi_n = k_s d$ is the phase difference introduced by the spoof SPP waveguide. The radiation pattern of each element is denoted by $f(\theta,\varphi)$, being considered as 1 since the beamwidth is wide. I_n is the excitation amplitude, being considered identical for all patches[S1]. From the related formula of scanning angle in the above, we can see that the propagation constant of SSPP transmission line (k_s) and the distance between two radiation units (d) are crucial parameters for scanning angle in Fig. S1(b). On the one hand, by manipulating the dispersion curve of the SSPP TL through structural parameters (e.g., the period of unit p and the thickness of the substrate), one is able to increase k_s at working frequencies so as to increase the scanning range. On the other hand, with a certain dispersion curve of the SSPP TL, the larger the distance (d) between the radiation elements, the larger the phase transition range with pure $n = -1$ harmonic in the fast wave area (within the light cone) will be, which may be more conducive to the expansion of the scanning angle. It is worth noting that this claim is only made to make the theoretical calculation much simpler. The theoretical calculation here is used to prove the beam scanning phenomenon, but not for the accurately calculation. With the equal amplitude assumption, the expression of the radiation pattern can be more concise. When calculating the efficiency in reality, the feeding amplitudes are different because of the leakage. The feeding amplitudes should become smaller as the wave propagation.

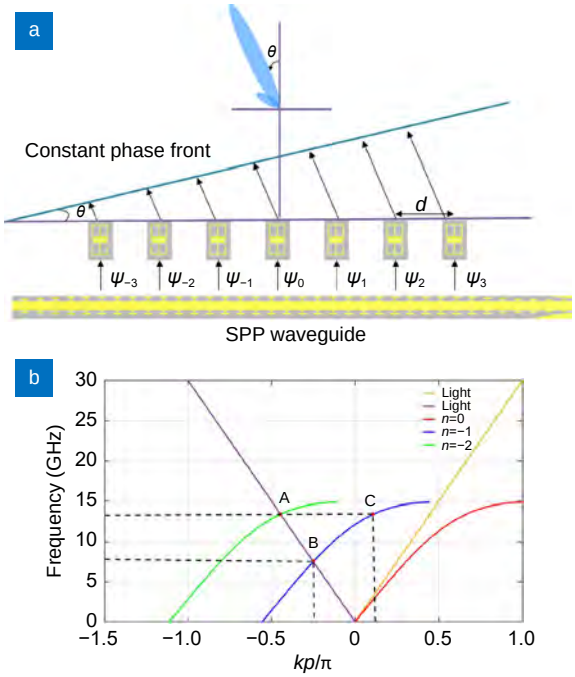

Fig. S1 | (**a**) Sketch of the feeding part of the proposed SSPPs-LWA. (**b**) Dispersion curves of space harmonics.

Section 2: "T"-shaped SSPP transmission line

The "T"-shaped structure is determined by bending the rectangular structures at both ends of the traditional "H"-shaped structure, as shown in Fig. S2(a). Through the simulation of the dispersion curve, it is found that "$a1$" and "$h1$" have a great influence on the dispersion characteristics, as given in Fig. S2(b, c), which can be analyzed by the equivalent circuit of the SSPPs unit.

After the SSPPs structure is determined, we adopt the method of transition from coplanar waveguide (CPW) to SSPPs TL for efficient excitation of SSPPs waves. The physical diagram of the SSPPs TL is shown in Fig. S2(d). Figure S2(e, f) show the test scenario of the SSPPs TL and the measurement results of the S parameters. It can be seen that the cutoff frequency is about 12 GHz, and the transmission coefficient (S_{21}) have a steep falling edge. The results show the S-parameters of the two substrates used, F4B (ε_r = 2.2, tanδ = 0.003, THK = 0.5 mm) with Taconic TLY-5 (ε_r = 2.2, tanδ = 0.0009, THK = 0.762 mm). It can be seen from the test results that Taconic TLY-5 has a higher transmission coefficient at high frequency (over 10 GHz). In the antenna design, we still choose Taconic TLY-5 as the substrate material. S_{21} will decrease at high frequencies, due to the incomplete match of the connectors, the dielectric loss, as well as the error caused by the test process and the environment. Nevertheless, the decrease is not significant, and the performance of the transmission line is verified in the test.

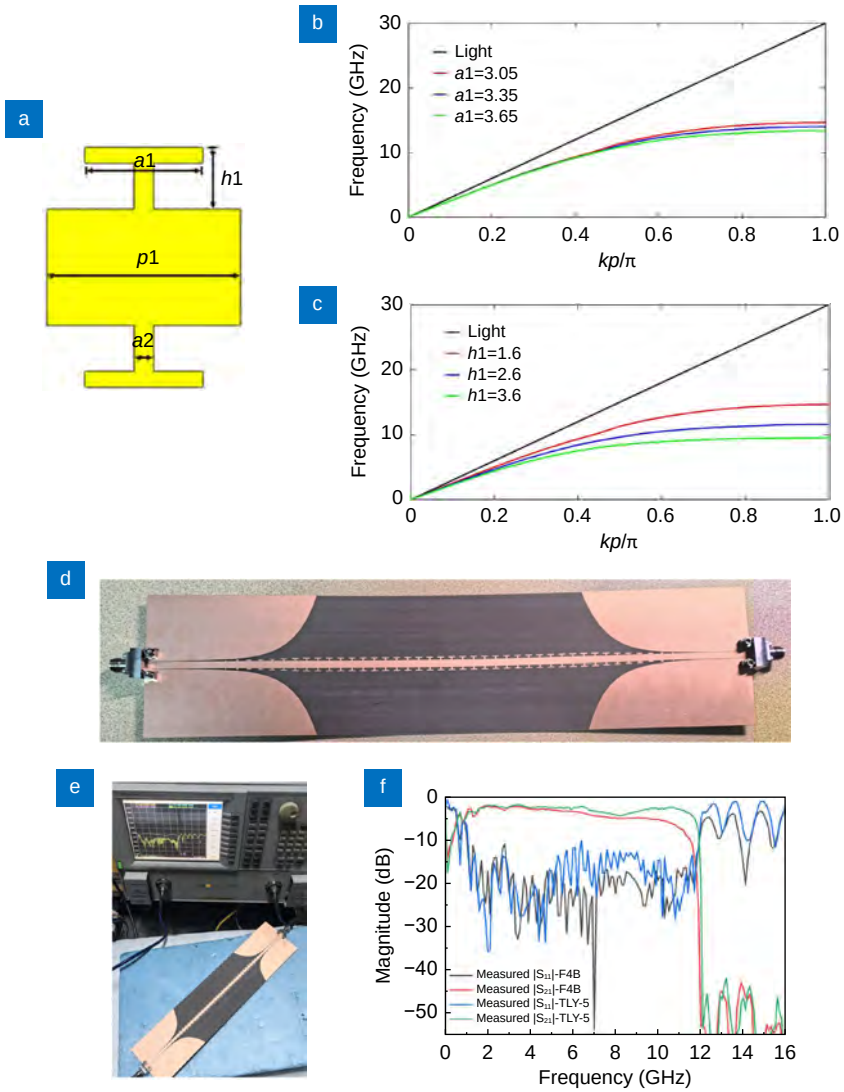

Fig. S2 | (**a**) "T"-shaped SSPPs structure, the dispersion curve of the "T"-shaped SSPPs structure with (**b**) parameter "a1" or (**c**) parameter "h1" changes. (**d**) Top views of the fabricated prototype of the proposed "T"-shaped SSPPs TL. (**e**) Test scenario. (**f**) Measured S-parameters results of two transmission line samples using F4B and Taconic TLY-5 as substrate, respectively.

Section 3: Design of the radiation unit

The radiation unit should consider how to set the topology circuit of the switch, that is, how to arrange the position of the PIN diode, and how to optimize the parameters to achieve the balance between the working bandwidth and the gain isolation. As shown in Fig. S3(c, d), the options of number of switches should consider the compromise between bandwidth and isolation. Series switch has the advantage of low transmission loss in a wide band, but its isolation is poor. Parallel switches are usually used in conjunction with 1⁄4 wavelength transmission lines, which are essentially narrow band, but have higher isolation than series. In addition, the use of two or more PIN diodes in series mode can improve the isolation, and the same bias current can be used in series to save power. It can also be seen that when the structure parameter "C" increases, and when the diode is disconnected, the transmission increases, which helps to optimize the isolation between the two states.

How to feed the PIN diode to complete the design of the bias circuit will affect the antenna radiation effect to a certain extent, here is to choose by punching metal holes to the back of the dielectric substrate to design. Firstly, the location of the bias circuit is selected. If the bias circuit line on the back of the dielectric substrate is arranged next to the corresponding radiation unit, on the one hand, due to the large amount of radiation units, it will make the copper line layout messy and cause interference, on the other hand, the current distribution on the radiation unit will lead to other po-

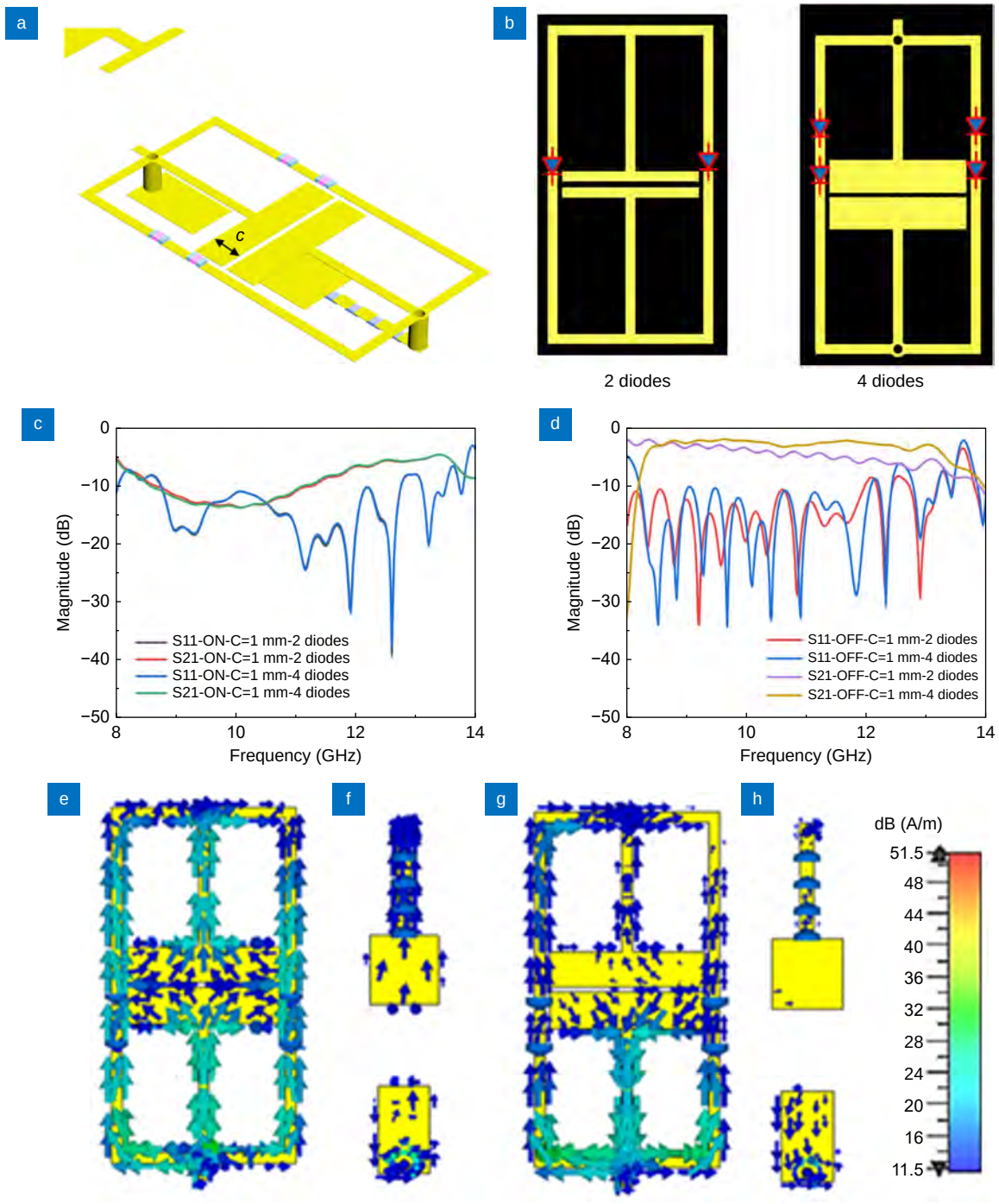

Fig. S3 | (**a**) Enlarged view of the radiation unit cell. (**b**) The radiation unit is loaded with 2 diodes or 4 diodes. When the diodes are all (**c**) OFF or (**d**) ON, simulated S_{21} of the smart SSPPs LWA at different working states with the period (c = 1.0 mm) are plotted. The current distribution of the radiation unit at 11 GHz. (**e**) The situation of the radiation unit during radiation state. (**f**) The condition of the radiation unit backfall feed line when the radiation state. (**g**) The situation of the radiation unit and (**h**) the feed line during the non-radiation state.

sitions, resulting in the difference in the effect of radiation. Therefore, the bias circuit line is arranged in the position corresponding to the radiation unit on the back of the dielectric substrate, making the wiring simple, no interference with each other, and the current distribution is still concentrated at the radiation unit, which has a small impact on the radiation effect. Secondly, the bias circuit structure must be continuously optimized during the design. On the one hand, it is necessary to ensure the effect of the two working states of the antenna, and on the other hand, consider whether the positive feeder terminal can be isolated from the radio frequency signal. The switching of an antenna work-

ing state can be judged by S-parameter and gain isolation, and the isolation of the radio frequency signal depends on the current distribution of the RF high-resistance line in the work frequency band. As shown in Fig. S3(e–h), Here is the current distribution at 11 GHz, it can be seen that no matter which working state is in, only little current flows through the radio frequency high-resistance line, as well as other frequency points in the working frequency band, so this design can achieve the effect of isolating the radio frequency signal.

Section 4: Equivalent circuit of PIN diode

In CST software simulation, we use the equivalent circuit of PIN diode to simulate the two states of the PIN diode. Usually, we can extract the equivalent circuit of PIN diode in ADS (Advanced Design System) software or from literatures. For the selection of PIN diode, the types and models of the PIN diode must be selected first. Among them, the first consideration is that the working frequency band of the PIN diode must meet the design requirements, and by replacing its equivalent circuit for simulation, combined with the actual cost and the ordering cycle of PIN diode, the MA4AGFCP910 model is finally determined. Its equivalent circuit diagram is shown in Fig. S4.

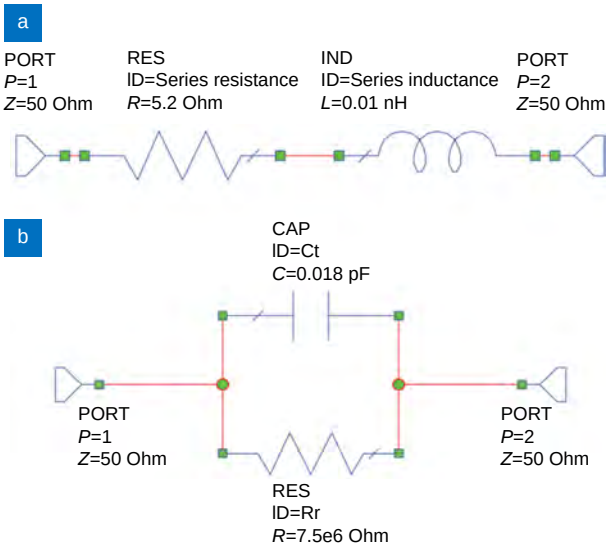

Fig. S4 | Equivalent circuit of a PIN diode (the pin diode we used) in two states: (**a**) on and (**b**) off.

It can be seen that in the "ON" state, the PIN diode is equivalent to a 5.2 Ω resistor in series with a 0.01 nH inductor; and in the "OFF" state, it is equivalent to a 7.5 MΩ resistor in parallel with a 0.018 pF capacitor. In the process of diode selection, we found that the smaller the value of equivalent capacitance in the "OFF" state, the higher the gain isolation.

Section 5: Test scenarios and results of the near electric field distribution

As for the near field test, a probe is set above the spoof surface plasmon polariton leaky-wave antennas (SSPP-LWA) to detect the near electric field and transfer data to the VNA through a low noise amplifier. Photo of the test scenario is shown in Fig. S5.

The measured results in Fig. S6 only contain the amplitudes of the electric field. We present the tested results for both the radiating and non-radiating states, at frequencies from 8.75 to 11.75 GHz. It can be observed that in the radiating state the amplitude of electric field begins to slowly decrease from the input port (the left side). Whilst in the non-radiating state, the energy is always transmitted efficiently along the SSPPs transmission line at the measured frequency points.

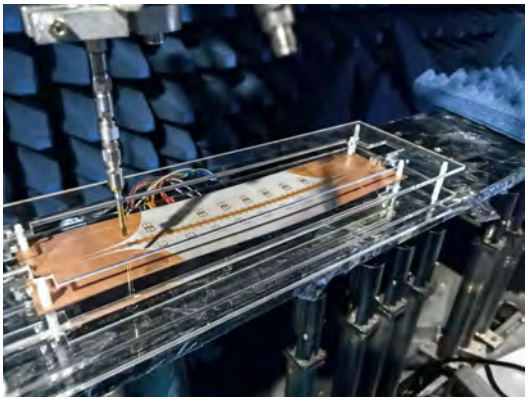

Fig. S5 | Photo of the near electric field test.

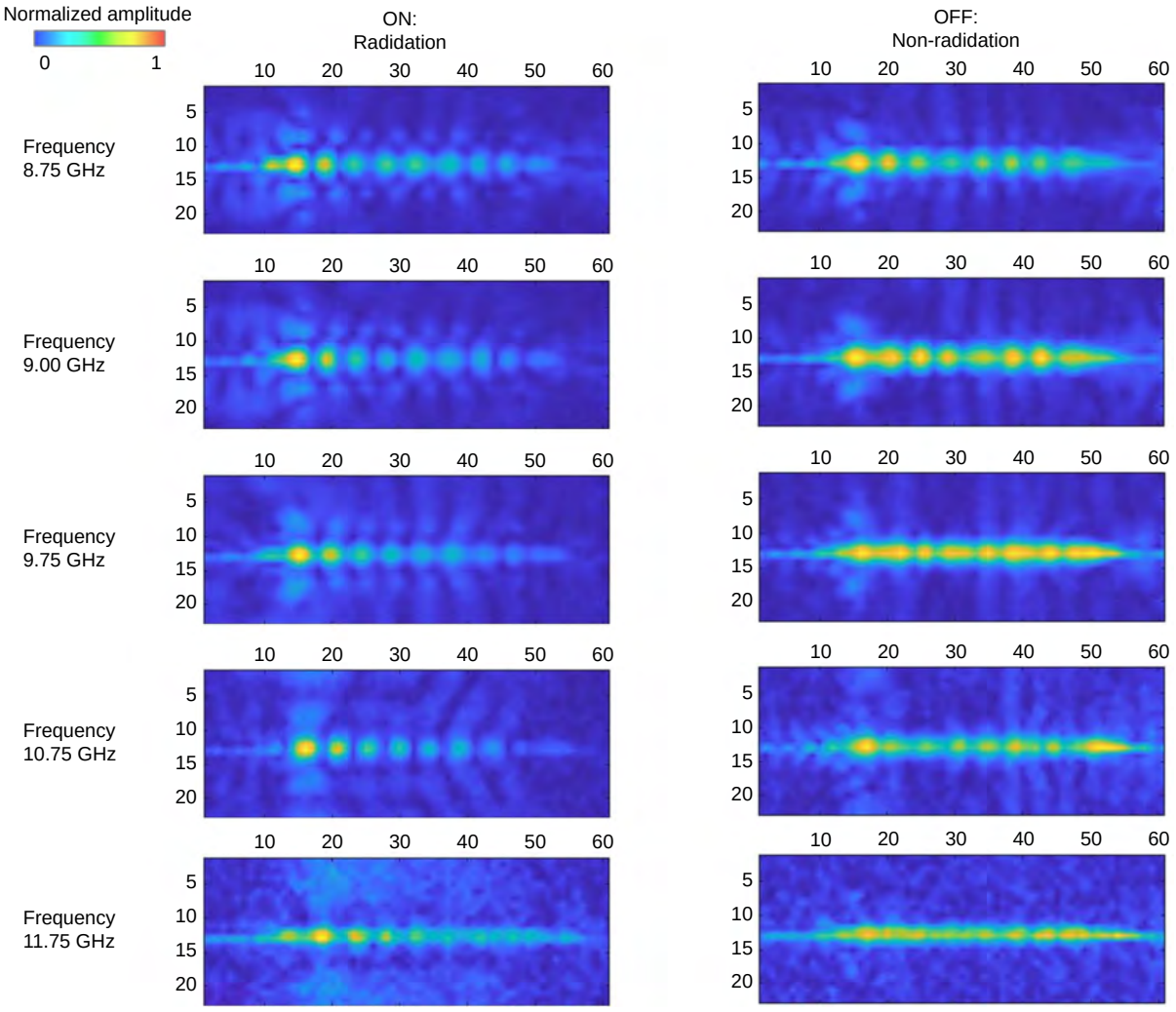

Fig. S6 | Measured near electric field distributions of the smart SSPP-LWA at 8.75 GHz, 9 GHz, 9.75 GHz, 10.75 GHz and 11.75 GHz in the radiating state and the non-radiating state, when the diode is "ON" or "OFF", respectively.

Section 6: Test scenarios of object detection switch of the SSPP-LWAs state

In the test scene, we use the model car instead of the jammer or other equipment as the target, and the blue area that can be photographed by the camera is the sight view. When we move the model car into or out of the target area, the smart antenna in Fig. S7(a) can also complete the quick switching of the working state, and achieve a more ideal external sensing function.

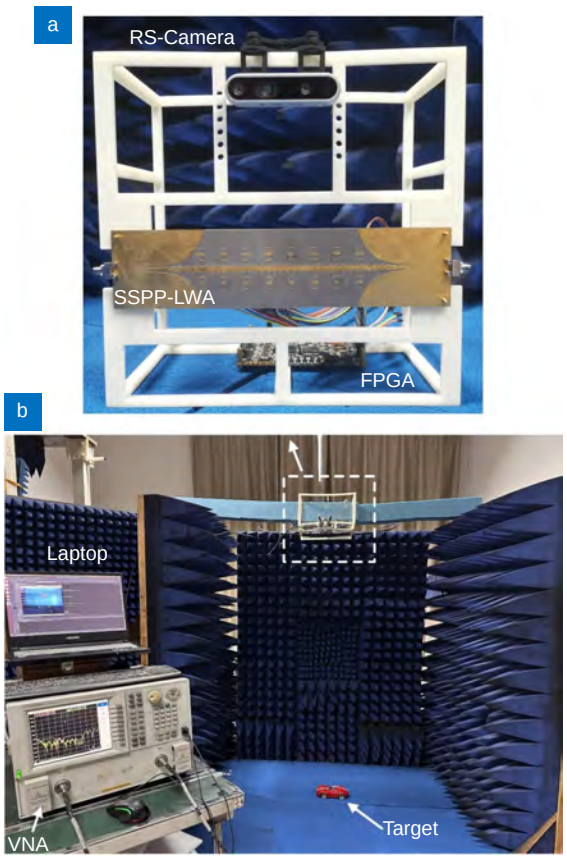

Fig. S7 | (**a**) A photo of the externally perceivable SSPP-LWA system. (**b**) The SSPP-LWA, FPGA and a vector network analyzer (VNA, Agilent N5230C) are set up in the chamber. The moving target is represented by one model car, which is captured by the RS-Camera. VNA is used to acquire the response data by measuring the S-parameters (S_{11} and S_{21}).

Figure S7(b) shows the construction of the test scenario, in which the blue area is the target area that can be captured by the camera. The photo also contains the VNA, FPGA, SSPP-LWA and the control system (a computer). When the model car moves to the target range we set, the FPGA output is low, the PIN diode on the smart SSPP-LWA is disconnected, and the antenna is in the transmission (non-radiating) state. When no model car appears within the target range, the FPGA outputs a high level and the PIN diode on the smart SSPP-LWA is "ON", and then the smart antenna is in the radiating state.

The SSPP-LWA can sense and automatically switch the working state quickly to avoid the influence of detectors or jammers and other devices within a certain range, and can ensure the safety of wireless communication in the airspace to a certain extent from the physical perception angle. It can be applied to the smart antenna technology for wireless communication security and physical layer security, and with reduced power consumption.

Section 7: Near-field test of the SSPP-LWA

The setups for measuring the scattering plane in the anechoic chamber are shown in Fig. S8. The incident wave is fed into the SSPP-LWA via coaxial cable. For measuring the scattering plane, a near-field probe is placed in the scanning plane 50 cm from the SSPP-LWA, and the measured area is 1200 × 480 mm^2. The measured results at different frequen-

Fig. S8 | The experimental setup for the measurement of the near field. The probe is 50 cm away from the SSPP-LWA, and scans in a plane of 700 × 500 mm² in the near field.

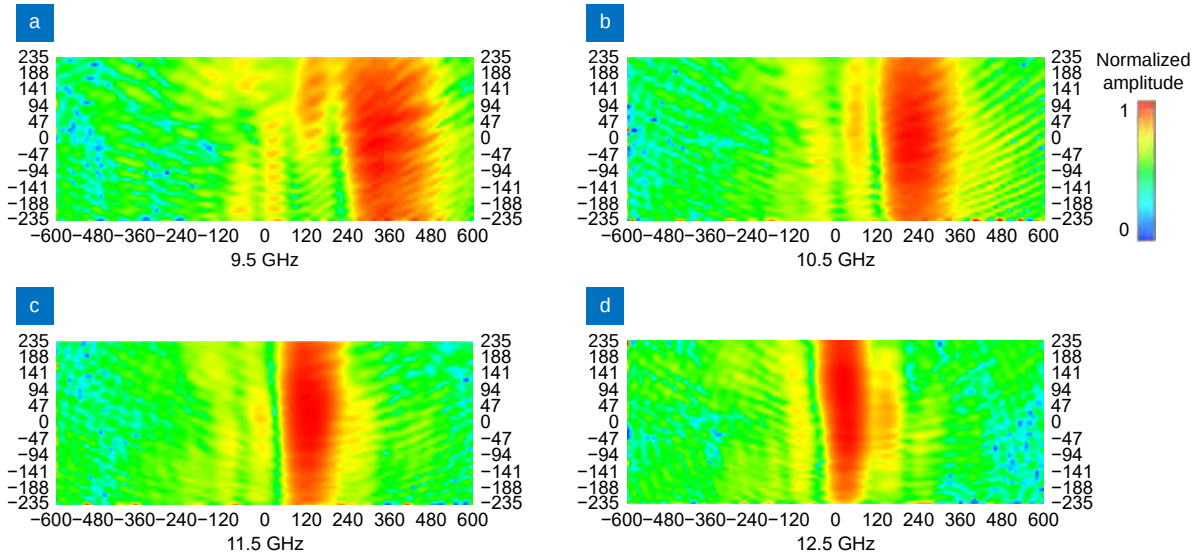

Fig. S9 | Measured amplitude of the near electric field.

cy are presented in Fig. S9, and it can be found that with the increase of frequency, the area with higher amplitude on the scanning plane shifts from left to right, once again verifying the effective beam scanning of the SSPP-LWA. The electric field diagram in the scanning plane is used to prove the basis of target tracking assisted by computer vision.

Section 8: Speed of the smart SSPP-LWA

We conducted measurements on the switching of the Field-Programmable Gate Array (FPGA) and the overall system, acquiring real-time data. As illustrated in Fig. S10(a), we use the camera to detect the target in real time, and the control system sends the voltage sequence to SSPP-LWA through FPGA. In the whole process, the camera collects the target every three frames and sends the voltage sequence once, which is to save energy. In addition, the voltage sequence used is random, which is convenient for the logic analyzer to collect the voltage on the pin. The FPGA pins were interfaced with a logic analyzer, while another computer was employed to monitor the logic analyzer results. Our findings revealed that the FPGA accomplished voltage transitions on the pins in response to the sequences with an approximate interval of 0.2 seconds, as depicted in Fig. S10(b). Analysis indicates that employing this strategy, the time required for each frame's processing by the FPGA amounts to approximately 80 milliseconds. Among them, the frequency switching speed of the signal source is about 20 ms, compared to 30 ms in the separate test process of the FPGA, and will no longer be tested. By reckoning, each frame is processed here, and the system reaction speed is about 80ms. Notably, the adoption of cameras featuring higher frame rates and computers boasting enhanced processing capabilities holds promise for further accelerating our system's responsiveness.

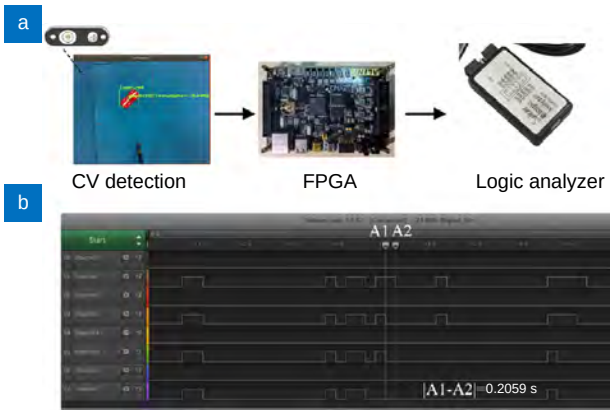

Fig. S10 | (**a**) Flow chart of speed detection. The computer vision completes the target detection, the control system sends instructions to the FPGA, and the FPGA detects the level change through the logic analyzer. (**b**) Results of the response speed of the SSPP-LWA system, when the coding sequence is sent every three frames.

References

S1. Yin JY, Ren J, Zhang Q et al. Frequency-controlled broad-angle beam scanning of patch array fed by spoof surface plasmon polaritons. *IEEE Trans Antennas Propag* **64**, 5181–5189 (2016).